Isotopic trends of nuclear surface properties of spherical nuclei

G. G. Adamian,[1] N. V. Antonenko,[1,2] H. Lenske,[3] S. V. Tolokonnikov,[4,5] and E. E. Saperstein[4,6]
[1]*Joint Institute for Nuclear Research, 141980 Dubna, Russia*
[2]*Mathematical Physics Department, Tomsk Polytechnic University, 634050 Tomsk, Russia*
[3]*Institut für Theoretische Physik der Justus–Liebig–Universität, D–35392 Giessen, Germany*
[4]*National Research Centre "Kurchatov Institute", 123182 Moscow, Russia*
[5]*Moscow Institute of Physics and Technology, 123098 Dolgoprudny, Russia*
[6]*National Research Nuclear University MEPhI, 115409 Moscow, Russia*
(Received 30 July 2016; revised manuscript received 29 September 2016; published 11 November 2016)

The density profiles of spherical nuclei are calculated with two methods based on the energy density functional approach. Isotopic trends are discussed in nuclear surface diffuseness. The simple parametrizations of the dependencies of nuclear diffuseness and radius on neutron number are suggested. The nucleus-nucleus potentials are calculated with the nucleon densities obtained and are compared with those resulting from the phenomenological treatment. The height of the Coulomb barrier is suggested to be used in the fit of the density-dependent nucleon-nucleon interaction.

DOI: 10.1103/PhysRevC.94.054309

I. INTRODUCTION

A challenge of nuclear theory is to propose an unified theoretical tool, applicable to the description of nuclear structure and nuclear reactions. *Ab initio* approaches [1,2] are just on this way. However, they are presently applicable to relatively light nuclei due to the computational limitations. So, the microscopic self-consistent theories based on the effective nucleon-nucleon forces with few phenomenological parameters are usually applied to describe the entire nuclear chart.

Historically, the Hartree–Fock (HF) method with effective Skyrme forces [3] or, a bit later, the one with Gogny forces [4] were the first such approaches. As an alternative the nuclear energy density functional (EDF) method was developed by Fayans with coauthors [5] which was generically related to the self-consistent theory of finite Fermi systems (TFFS) [6]. The generalizations of the HF approach with effective forces for superfluid nuclei were formulated first as the HF + BCS method and later, as a more general Hartree–Fock–Bogoliubov (HFB) method. As for the Fayans EDF method, it was from the beginning formulated for superfluid nuclei, with the EDF depending on the normal and anomalous densities. Nowadays the above HF methods with the effective force are usually formulated as the EDF method with Skyrme or Gogny functionals; see Ref. [7] and references therein. The same is true, to some extent, for the relativistic mean-field theory which became popular last decade; see e.g., Refs. [8–10].

There are partially *ab initio* microscopic approaches in which the main part of the EDF parameters is found starting from the free NN interaction and only several phenomenological parameters are introduced, significantly less than in the case of the EDFs which are completely phenomenological. Thus, the $M3Y$ representation of the G matrix from the Paris NN was used in Ref. [11] as a starting point for finding the effective NN interaction. It was modified by introducing density-dependent vertex renormalizations, with the use of several phenomenological parameters. More recently, the so-called Bolognia–Catania–Paris–Madrid method was developed [12,13], based on the EDF of nuclear matter found within the Brueckner–Hartree–Fock method from the Argonne AV18 force. Only three phenomenological parameters were introduced; two for the surface and one for the spin-orbit components.

The crucial test of the phenomenological theory is the description of the ground-state properties of nuclei as the binding energies, radii, equilibrium deformations, and decay properties. The theory has to predict the low-lying excited states as well. For nuclear reactions, one should have a tool to calculate the nucleus-nucleus potential as the main ingredient of description of all reaction processes. The parameters of the EDFs are usually fit to the ground-state nuclear characteristics. The use of them for description of nuclear reactions provides an important additional test. Indeed, the nucleus-nucleus potential is mainly defined by the effective NN forces at low nuclear density (their external part), while the ground-state nuclear properties are mainly determined by the NN interaction in the nuclear interior (the internal part). An example of the test of the EDF method in description of reactions induced by heavy ions is one of the goals of this work.

Average central densities, nuclear radius, and surface diffuseness are basic quantities characterizing finite nuclear systems. Extensive discussions are currently made on the proton-neutron differences of proton-neutron nuclear radii and diffuseness to study the symmetry energy [14–20]. The polarization of the nuclear surface in the deformed nuclei was also considered in Ref. [21]. Here, we focus on the isotopic trends of nucleon distributions considering all studied nuclei as spherical. A particular attention is taken to study the diffuseness of the surface which has an important impact on the calculation of the Coulomb barrier [22–24] in the nucleus-nucleus potential. While the central density and radius are mainly related to the internal NN forces, or to the properties of nuclear matter, the diffuseness of the nuclear surface turns out to be related to the external part of these forces, being the effect of finite Fermi systems. The nuclear surface region is of particular importance for nuclear reactions. From point of

view of nuclear dynamics, this is a transitional region where the in-medium interactions gradually undergo into the free NN interactions. The TFFS [25], for example, accounts for these transient effects explicitly introducing internal and external interactions.

The article is organized as follows: in the next section, the two versions of the EDF method to characterize nuclear shapes and density profiles are exposed. The first one is partially *ab initio* EDF [11]. The Fayans EDF [5,26,27], which is completely phenomenological, is the second one. Section III provides an analysis of the density profile and its consequence in the calculation of nucleus-nucleus potential. In Sec. IV, an example of consequences on nuclear dynamics is given.

II. ENERGY DENSITY FUNCTIONAL APPROACH TO NUCLEAR GROUND-STATE DENSITY DISTRIBUTIONS

A. Method I: Partially *ab initio* energy density functional

Nuclear binding energies, single-particle states, and ground-state densities are described by an EDF:

$$\mathcal{E}(\rho,\tau,\kappa) = \mathcal{E}_{\rm kin}(\tau) + \mathcal{E}_{\rm int}(\rho) + \mathcal{E}_{\rm pair}(\rho,\kappa) - \sum_{q=p,n} \lambda_q \rho_q, \quad (1)$$

given by the kinetic-energy density $\mathcal{E}_{\rm kin}$, the interaction energy density $\mathcal{E}_{\rm int}$, and the pairing interaction density $\mathcal{E}_{\rm pair}$. The functional $\mathcal{E}$ depends on the proton and neutron densities $\rho = \{\rho_p,\rho_n\}$, the corresponding kinetic energy densities $\tau = \{\tau_p,\tau_n\}$, and the pairing densities $\kappa = \{\kappa_p,\kappa_n\}$. To enforce particle number conservation, the proton and neutron chemical potentials $\lambda_{p,n}$ are introduced. The interactions contained in $\mathcal{E}_{\rm int}$ and $\mathcal{E}_{\rm pair}$ are derived from in-medium G-matrix interactions which is supplemented by an effective three-body interaction in order to describe properly the saturation properties of infinite nuclear matter. Following the density matrix expansion scheme [28] as used in Ref. [11] an effective density dependent local two-body interaction is constructed, incorporating already antisymmetrization. Hence, our approach is based effectively on an energy density functional with

$$\mathcal{E}_{\rm kin}(1,2) = \sum_{q=p,n} \tau_q(1,2), \quad (2)$$

$$\mathcal{E}_{\rm int}(1,2) = \frac{1}{2}[\rho^\dagger(1)V_{00}(1,2)\rho(2) + \rho_1^\dagger(1)V_{01}(1,2)\rho_1(2)] + \mathcal{E}_C(1,2) + \mathcal{E}_{\rm s.o.}(1,2) + \mathcal{E}_{\rm res}(1,2), \quad (3)$$

$$\mathcal{E}_{\rm pair}(1,2) = \frac{1}{2}\sum_{q=p,n} \kappa_q^\dagger(1)V_{qq}(1,2)\kappa_q(2), \quad (4)$$

where V_{00} and V_{01} denote the interaction form factors in the isoscalar and isovector interaction channels which for spin-saturated nuclear systems have nonzero ground-sate expectation values. V_{qq} indicates the paring interaction for protons and neutrons, respectively, taken here as the contact interaction with the strength fixed by the singlet-even on-shell scattering matrix at the local Fermi momentum $k_q = k_{F_q}(\rho_q)$. All interaction form factors depend on the density as discussed in Ref. [11]. Residual interactions, which do not contribute to the ground state of a spin-saturated nucleus, are contained in $\mathcal{E}_{\rm res}$. In addition, in a finite nucleus also the Coulomb and spin-orbit densities are given in terms of the charge density ρ_c and the spin-orbit energy density $\rho_{\rm s.o.}$:

$$\mathcal{E}_C(1,2) = \frac{1}{2}e^2\rho_C^\dagger(1)\tilde{V}_C(1,2)\rho_C(2), \quad (5)$$

$$\mathcal{E}_{\rm s.o.}(1,2) = \frac{1}{2}\sum_{T=0,1} W_T(1,2)\mathbf{J}_T^\dagger(1)\nabla\rho_T(2) + \text{H.c.}, \quad (6)$$

where the interaction $\tilde{V}_C$ accounts for antisymmetrization effects which we treat in local density approximation with an effective density-dependent contact interaction. The spin-orbit energy density is defined in terms of the isoscalar and isovector interactions W_T and the corresponding spin-currents $\mathbf{J}_T$. The isoscalar and isovector densities are given in terms of the proton and neutron ground state as

$$\rho = \rho_n + \rho_p \text{ and } \rho_1 = \rho_n - \rho_p, \quad (7)$$

respectively.

The kinetic, nucleon, and pairing densities are defined in terms of single-particle wave functions φ_{qjm}, occupation probabilities $n_{jm} = v_{jm}^2$, and the emptiness $u_{jm}^2 = 1 - v_{jm}^2$:

$$\tau_q = \sum_{jm} v_{jm}^2 \frac{\hbar^2}{2m_q}|\nabla\varphi_{qjm}|^2, \quad (8)$$

$$\rho_q = \sum_{jm} v_{jm}^2|\varphi_{qjm}|^2, \quad (9)$$

$$\kappa_q = \frac{1}{2}\sum_{jm} u_{jm}v_{jm}|\varphi_{qjm}|^2. \quad (10)$$

The isospin spin-currents are given by

$$\mathbf{J}_T = \sum_{q,jm} v_{qjm}^2\varphi_{qjm}^\dagger\boldsymbol{\tau}^T[-i\nabla\times\boldsymbol{\sigma}]\varphi_{qjm}. \quad (11)$$

In a spherical nucleus, only the radial projection $J_{rT} = \mathbf{r}\mathbf{J}_T$ contributes effectively,

$$J_{rT} = \sum_{q,jm} v_{qjm}^2\varphi_{qjm}^\dagger\boldsymbol{\tau}^T\boldsymbol{\ell}\cdot\boldsymbol{\sigma}\varphi_{qjm}, \quad (12)$$

which is seen to describe the spin-orbit density. The charge density $\rho_c(k)$ is obtained by folding the proton and neutron densities (9) by the corresponding proton and neutron charge form factors, respectively, taken from the experiment [29,30].

Variation of $\mathcal{E}$ with respect to $\varphi_{qjm}^\dagger$ leads to the equations for the single-particle wave functions

$$\left(-\frac{\hbar^2\nabla^2}{2m_q} + U_q + e_qU_C + U_{\rm s.o.}\boldsymbol{\ell}\cdot\boldsymbol{\sigma} + \Delta_q - \varepsilon_{qj}\right)\varphi_{qjm} = 0, \quad (13)$$

with the single-particle self-energy

$$U_q = \frac{\delta}{\delta\rho_q}(\mathcal{E}_{\rm int} + \mathcal{E}_{\rm pair}), \quad (14)$$

which accounts for isoscalar and isovector contributions and includes rearrangement self-energies due to the intrinsic density dependence of the interactions [31]. The pairing

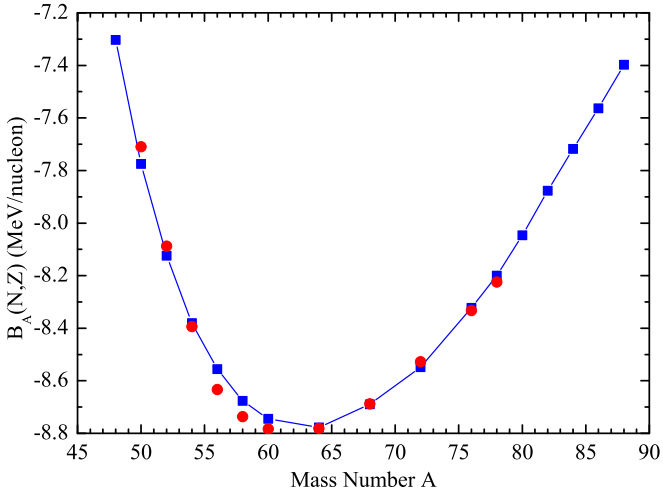

FIG. 1. The binding energies per nucleon for the Ni isotopic chain. The energy density functional results (solid squares connected by lines) are compared with the experimental data (solid circles) of Ref. [33].

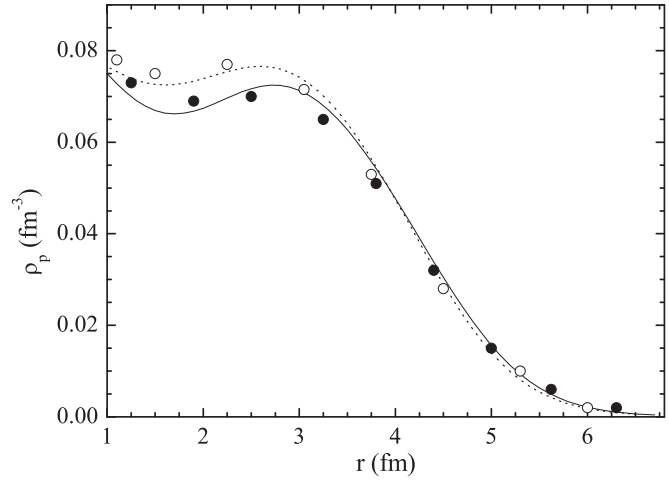

FIG. 2. The calculated radial distributions of the proton density ρ_p for ^{58}Ni (dotted line) and ^{64}Ni (solid line) are compared with the experimental data [37] shown by open and solid symbols, respectively.

field is

$$\Delta_q = \frac{\delta}{\delta\kappa_q}\mathcal{E}_{\rm pair} \sim V_{qq}(\rho_q)k_q, \tag{15}$$

where we neglect higher-order corrections from the variation of the state-dependent gaps, which are defined by the matrix elements $\Delta_{qj} = \langle qjm|\Delta_q|qjm\rangle$ of the pairing field and determine the quasiparticle energies and occupation numbers in BCS approximation. In a spherical nucleus they are independent of the magnetic quantum numbers and, thus, are given as

$$E_{qj} = \sqrt{(\varepsilon_{qj} - \lambda_q)^2 + \Delta_{qj}^2}, \tag{16}$$

$$v_{qj}^2 = \frac{1}{2}\left(1 - \frac{\varepsilon_{qj} - \lambda_q}{E_{qj}}\right). \tag{17}$$

Solving Eqs. (13) with the parameters defined in Ref. [11], we find the nucleon density profile with Eq. (9). Equation (13) is solved by direct numerical integration. For that purpose the Numerov–Cowell method (see, e.g., Ref. [32]), is a stable and fast algorithm optimized for the solution of ordinary second-order differential equations. In practice, the eigenvalue problem is solved by matching outward and inward integrated solutions by variation of ε_{qj} until both solutions and their first derivatives are smoothly connected. In comparison to the widely used expansion in terms of oscillator wave functions, our approach avoids artificial cutoff effects and guarantees the correct exponential falloff of bound-state wave functions and densities in the asymptotic region up to arbitrarily large radii. Also particle states will be described with the proper asymptotic oscillatory behavior.

The energy density functional approach leads to good description of nuclear binding energies (Fig. 1). The experimentally available data [33] are well reproduced. The slight deviations around ^{56}Ni are most likely due to the neglect of the rank-2 tensor interactions which have been found to add a non-negligible amount of energy to the total binding energies around subshell closures in even-even nuclei in this mass region [34]. Further results on the ground-state properties and nuclear excitations of beta-stable and exotic nuclei were presented in Refs. [11,35,36]. Here, in Fig. 2 we demonstrate a good description of the measured [37] charge-density distribution for ^{58,64}Ni. As seen, the quality of description of the characteristics of proton density distribution is similar to those in Refs. [9,17–20].

B. Method II: Phenomenological Fayans energy density functional

As an alternative approach we use the phenomenological EDF by Fayans [5,26]. For completeness, we describe in short its main peculiarities. In more detail, this EDF is presented in Ref. [26] or in more recent Refs. [38,39]. The Fayans EDF belongs to the class of finite-range functionals with Yukawa-type coordinate dependence of the central force. The ground-state energy of a nucleus is considered as a functional of normal ρ and anomalous κ densities. The normal part of the EDF $\mathcal{E}_{\rm norm}$ contains the central, spin-orbit and effective tensor nuclear terms and Coulomb interaction term for protons. The in-volume central term can be schematically written as

$$\mathcal{E}^{\rm v}_{\rm norm}(x) = \frac{C_0 F_{ex} x^2}{2}\frac{1+\alpha x^\sigma}{1+\gamma x}, \tag{18}$$

where $x = \rho/\rho_0$ is the relative density, whereas F_{ex}, σ and γ are the parameters. $C_0 = (dn/d\varepsilon_{\rm F})^{-1} = \pi^2/mp_{\rm F}$ is the usual TFFS normalization factor, inverse density of states at the Fermi surface. The isotopic indices are omitted for brevity. The corresponding term of the Skyrme EDF can be obtained from Eq. (18) putting $\gamma = 0$, thus reducing the "Fayans denominator" to unity. The use of the bare mass instead of the effective one, $m^* = m$, is another peculiarity of the Fayans method. Both the peculiarities of the Fayans EDF reflect, in a hidden form, the energy dependence effects inherent to the

self-consistent TFFS [6]. In particular, the effective mass is close to the bare mass in the self-consistent TFFS due to almost exact cancellation of two effects: of the energy and momentum dependence of the nucleon mass operator. The surface part $\mathcal{E}^{s}_{norm}(x)$ of the normal EDF is derived from the expression of Eq. (18) type (with different values of parameters) by action of the operator

$$D(\mathbf{r}-\mathbf{r}') = \frac{1}{4\pi r_c^2 r}\exp\left(-\frac{r}{r_c}\right) - \delta(\mathbf{r}-\mathbf{r}'). \quad (19)$$

Evidently, the surface term $\mathcal{E}^{s}_{norm}(x)$ vanishes in nuclear matter, $x \equiv 1$.

The anomalous Fayans EDF in Ref. [26] was used in the form of

$$\mathcal{E}_{an}(\mathbf{r}) = \sum_{\tau} \mathcal{F}^{\xi,\tau\tau}(\mathbf{r};[\rho])|\kappa^{\tau}(\mathbf{r})|^2, \quad (20)$$

with the three-parameter effective pairing interaction:

$$\mathcal{F}^{\xi} = C_0 f^{\xi} = C_0\left[f^{\xi}_{ex} + h^{\xi}x^{2/3} + f^{\xi}_{\nabla} r_0^2(\nabla x)^2\right]. \quad (21)$$

The first two terms of Eq. (21) are usual for the TFFS [25] or modern Skyrme HFB EDFs [7], whereas the third one, $\propto(\nabla x)^2$, was introduced in Ref. [40]. The latter turned out to be of the principal importance for reproducing the odd-even staggering effect in charge radii of several long isotopic chains (Ca, Sn, and Pb), including the cases of negative isotopic shifts [26]. In Ref. [26], the EDF DF3 was used with the set of parameters fit to the equation of state of nuclear and neutron matter by Friedman–Pandharipande [41] and masses and radii of spherical nuclei, from calcium to lead. Later, in Ref. [27], the spin-orbit and effective tensor components of this EDF were modified to describe nuclei heavier than lead. The corresponding EDF, named DF3-a, turned out to be successful in describing uranium and transuranium nuclei without spoiling the accuracy of description of lighter nuclei. In fact, method II allows us to describe successfully the ground-state properties of nuclei from the calcium region to the transuranium one. In particular, the charge radii are reproduced with this functional with the perfect accuracy of 0.01–0.02 fm [39]. Method II was proved out to be also successful in systematic description of nuclear magnetic [42,43] and quadrupole [38,44,45] moments. The energies and $B(E2)$ values for the first 2^+ excitations in semimagic nuclei [38,46] is another example of successful application of the Fayans EDF. A record accuracy was reached also [47] in describing the single-particle energies of seven doubly magic nuclei.

In the calculation of nucleus-nucleus potentials we parametrize the self-consistent density distributions found with method II by properly normalized Fermi functions. Quality of fitting is demonstrated in Sec. III. It should be stressed that the tails of the density distributions mainly contribute to the folding integral containing in the expression for the nuclear part of nucleus-nucleus potential. Therefore, the differences between the self-consistent density distributions and the Fermi ones, which are seen in the central regions, are expected to unimportant for the results.

III. CALCULATED RESULTS

A. Nucleon density distribution

The nucleon density distribution ρ in the spherical nucleus is usually taken in the three-parameter symmetrized Fermi-type form:

$$\rho(r) = \frac{\rho_0}{1+\exp[(r-R)/a]}, \quad (22)$$

where ρ_0 is the saturated nucleon density in the center of the nucleus, $R = r_0 A^{1/3}$ is the nuclear radius with the parameter r_0, and a is the nuclear diffuseness. As seen in Fig. 3, one can fit well the density profile with Eq. (22). The value of

$$\rho_0 = \frac{3}{4\pi r_0^3}\frac{1}{1+\left(\frac{\pi a}{r_0 A^{1/3}}\right)^2}, \quad (23)$$

provides the proper normalization of Eq. (22). By using the values of r_0 and a obtained in a three-parameter fit of the nuclear density profile in Fig. 3, we obtain from Eq. (23) $\rho_0 =$ 0.158, 0.162, 0.156, and 0.154 fm^{-3} for ^{64}Ni, ^{122}Sn, ^{196}Pb, and ^{276}Ds, respectively. These values of ρ_0 differ from those of the three-parameter fit (Fig. 3). So the three-parameter fit provides $\rho(r)$ which is not normalized to the total number of nucleons. By using ρ_0 from Eq. (23), we fit the nucleon density profile with r_0 and a and obtain the normalized $\rho(r)$. As seen in Fig. 3, the values of ρ_0 obtained in this way are close to 0.16 fm^{-3}, which resulted from consideration of infinite nuclear matter, and the variation of ρ_0 has minor influence the tail of the density distribution. To reveal the isotopic trends in r_0 and a and simplify the calculations of nucleus-nucleus potential, one can take safely $\rho_0 = 0.16$ fm^{-3} up to an accuracy of a few percent and consider the fit of the density profile with r_0 and a. Taking this ρ_0, we focus on the quality of the description of the nucleon density distribution at $r > 0.8R$ (Fig. 3). Because the nuclear density tail is mainly responsible for the nucleus-nucleus interaction, the quality of the nuclear structure input can be checked in the calculation of the nucleus-nucleus potential. Indeed, the height of the Coulomb barrier is a measurable value.

If we fix the values of $\rho_0 = 0.16$ fm^{-3} and $r_0 = 1.15$ fm, the description of the density tail becomes worse (Fig. 3), particularly in the case of light nuclei. In a heavy nucleus, the density profile can be well fit even at fixed ρ_0 and r_0.

For further consideration, we use the two-parameter fit and set $\rho_0 = 0.16$ fm^{-3} because this value is close to that obtained in the two-parameter fit, which resulted in the normalized $\rho(r)$. If the value of ρ_0 is fixed in Eq. (22), the fit of nucleon-density profile results in smoother dependence of a on N. Although the values of a are slightly larger in this fit, the qualitative dependence on N remains.

We found that r_0 is weakly dependent on the neutron number of nucleus. Based on the calculations of nucleon density profiles, the parametrization

$$r_0 = Z^{1/37}\ (\text{fm}) \quad (24)$$

is suggested to estimate the radius parameter. In accordance with Eq. (24), the value of r_0 varies from 1.07 fm for Mg to 1.135 fm for Ds. Note that this unusual expression provides

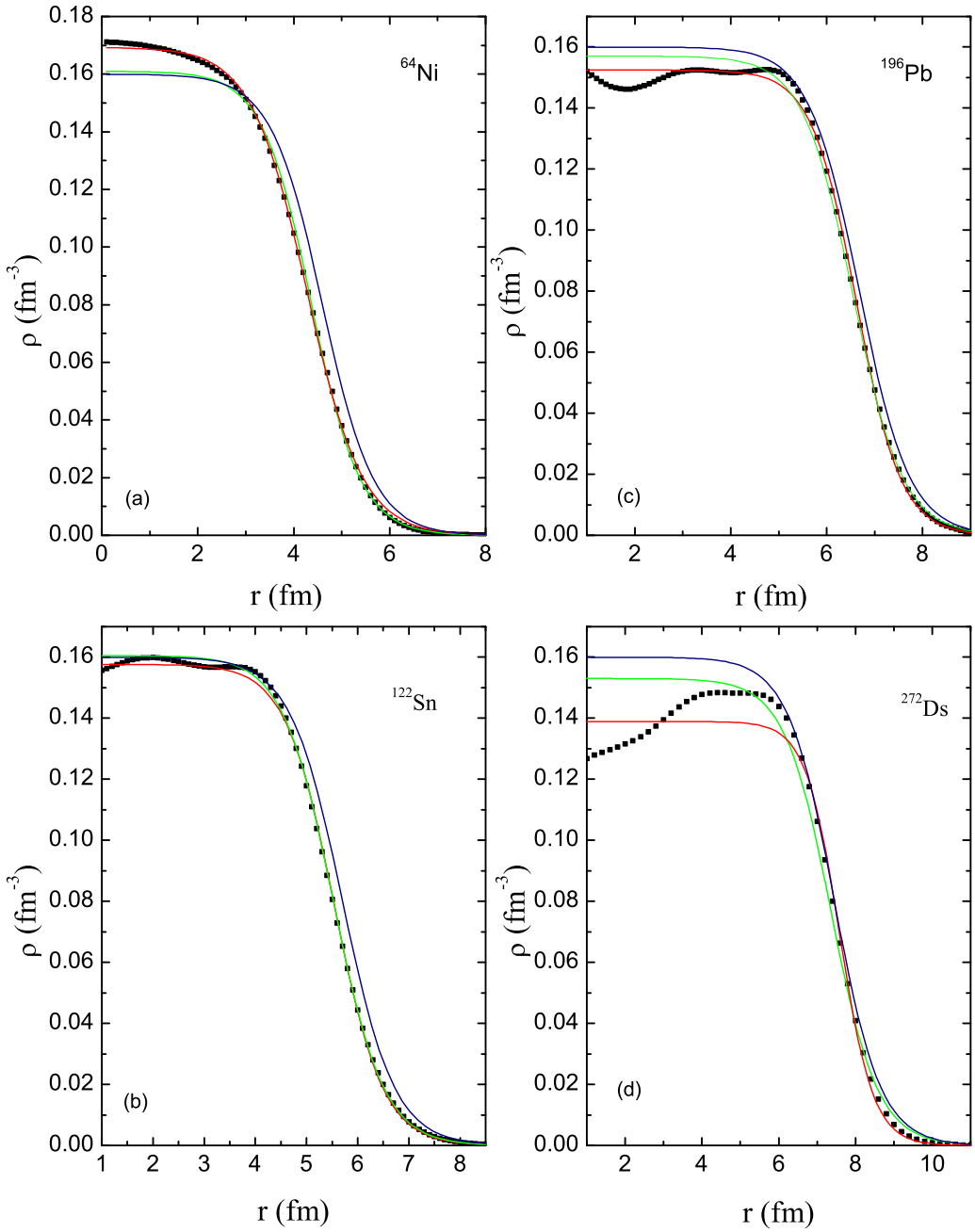

FIG. 3. The nucleon-density distributions calculated with method I in indicated spherical nuclei are fit with Eq. (22). The results of the three-parameter fit are shown by red lines. The results of the two-parameter fit at ρ_0 defined from Eq. (23) are shown by green lines. The results of the one-parameter fit at fixed $\rho_0 = 0.16$ fm^{-3} and $r_0 = 1.15$ fm are shown by blue lines.

the values of r_0 close to those from more sophisticated parametrization given below.

In Figs. 4 and 5, the isotopic dependencies of the diffuseness a in Eq. (22) are shown. The present results and those obtained in Ref. [21] demonstrate the same qualitative dependence on the neutron number. The diffuseness is minimal at $N = 28$ and 50, corresponding to the magic numbers. As in Ref. [48], the $a(N)$ dependence in Pb is essentially nonlinear and is characterized by an increase with N from 112–116 to 126 (Fig. 5). The value of a depends on the strength of NN forces at small nucleon density. This strength is mainly defined by the external NN interaction. The density dependence of NN forces influences the diffuseness as well. As shown, various NN interactions or energy-density functionals provide a good description of nuclear properties but result in quite different values of a. In Figs. 4 and 5, the values of a calculated within different methods vary within a factor of 1.2. In Ref. [9], the diffuseness parameter for Ni is essentially a step function: $a \approx 0.45$ fm for $N < 40$ and $a \approx 0.5$ fm for larger N. Although the values of a are close to those obtained in Ref. [9], the qualitative dependence on N is rather different, which reflects the dependence of a on the nucleon-nucleon interaction used.

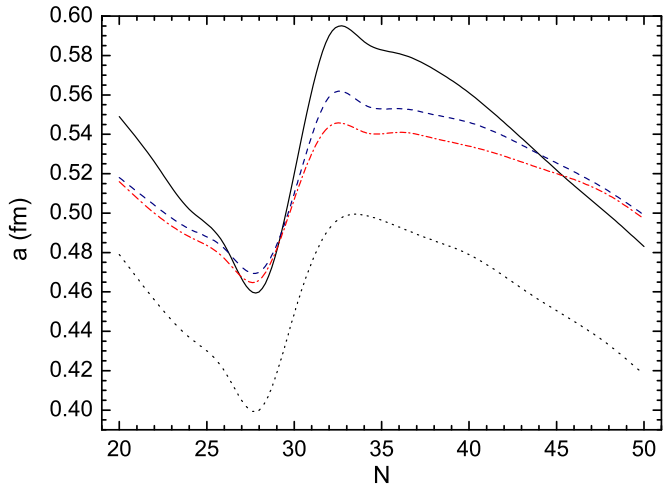

FIG. 4. The comparison of isotopic dependencies of diffuseness of Ni obtained with method I (solid line), method II (dotted line), and the approach of Ref. [21] (dashed and dash-dotted lines result from the SLy4 and SKMS interactions, respectively).

Based on the calculations of proton and neutron densities, the expressions

$$R_p = 1.249A^{1/3} - 0.5401 - 0.9582\frac{N-Z}{A}\ (\text{fm}),$$
$$R_n = 1.2131A^{1/3} - 0.4415 + 0.8931\frac{N-Z}{A}\ (\text{fm}),$$
$$a_p = 0.4899 - 0.1236\frac{N-Z}{A}\ (\text{fm}),$$
$$a_n = 0.4686 + 0.0741\frac{N-Z}{A}\ (\text{fm}) \qquad (25)$$

can be suggested to estimate the proton R_p and neutron R_n radii as well as the diffuseness for protons a_p and neutrons a_n. These expressions are suitable for estimating the smooth part of isotopic dependence of nuclear radius and diffuseness. As seen in Fig. 6, the nuclear radii for protons and neutrons are well reproduced. The proton (neutron) diffuseness is rather

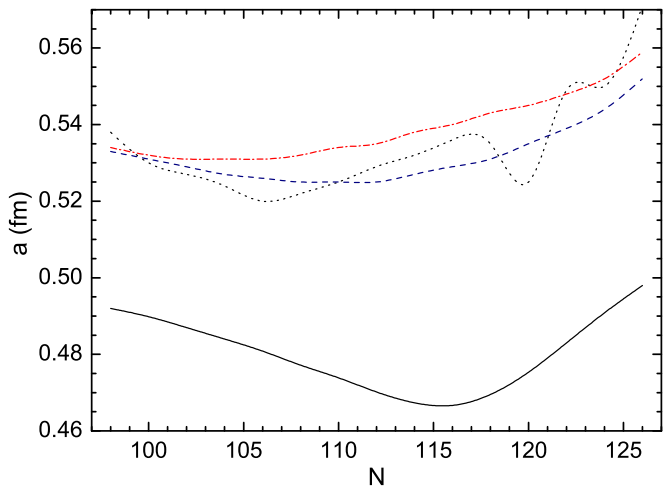

FIG. 5. The same as in Fig. 4, but for Pb.

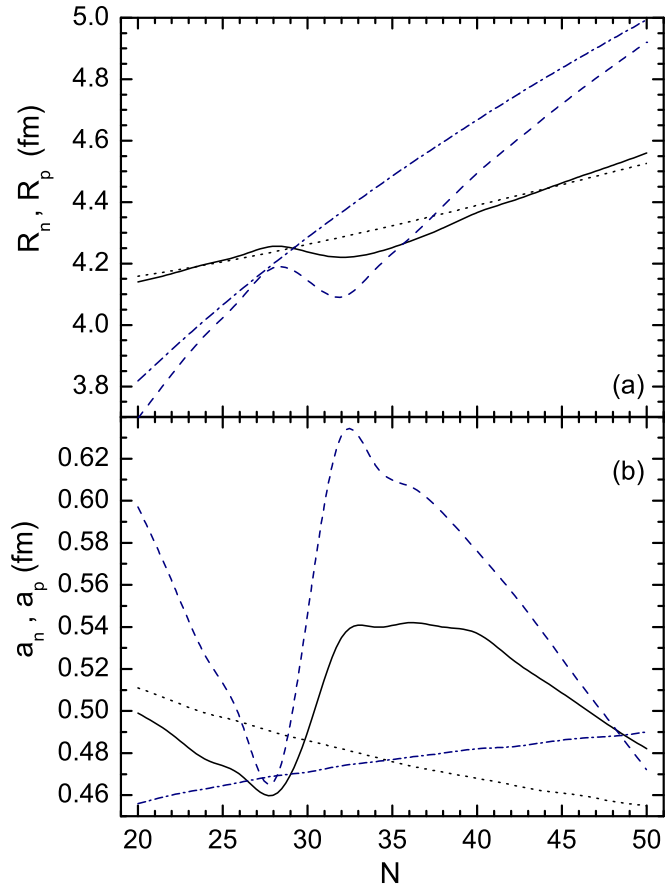

FIG. 6. Comparison of isotopic dependencies of (a) proton (solid line) and neutron (dashed line) radii, and (b) proton (solid line) and neutron (dashed line) diffuseness obtained with method I for Ni isotopes with those calculated for protons (dotted lines) and neutrons (dash-dotted lines) with Eqs. (25).

well described for the nuclei with N near the magic values. The nuclear radius is estimated as $R = (ZR_p + NR_n)/A$ that results in $r_0 = 1.10$–1.12 fm for the Ni isotopes considered. The expression (24) leads to $r_0 = 1.1$ fm. As seen, the addition dependence of r_0 on N in Eq. (25) causes about 2% correction to the value of r_0 obtained with Eq. (24).

As seen in Figs. 7–11, the diffuseness calculated with the methods I and II are different. Method I provides larger a for Ni and Mg. However, it results in smaller values of a for Pb and Ds than those from method II. Although Mg isotopes are well deformed in the ground state, here we consider them as spherical to reveal the isotopic trend of the diffuseness without polarization effects caused by deformation [21]. For Ni and Sn, the functions $a(N)$ have the minima at $N = 28$, 50, and 82. There is also the minimum of a at $N = 162$–164 in Ds. In the single-particle schemes of spherical nuclei, these neutron shells and subshells are closed by the levels with large orbital angular momenta ($l \geqslant 7$) [49]. Thus, the centrifugal barrier restricts the diffuseness of some closed-shell nuclei. For Mg and Pb, the magic neutron numbers $N = 20$ and 126 are not reflected in the $a(N)$ dependence because these shells are closed by the levels with small orbital angular momenta. So one can conclude that the last occupied single-particle level

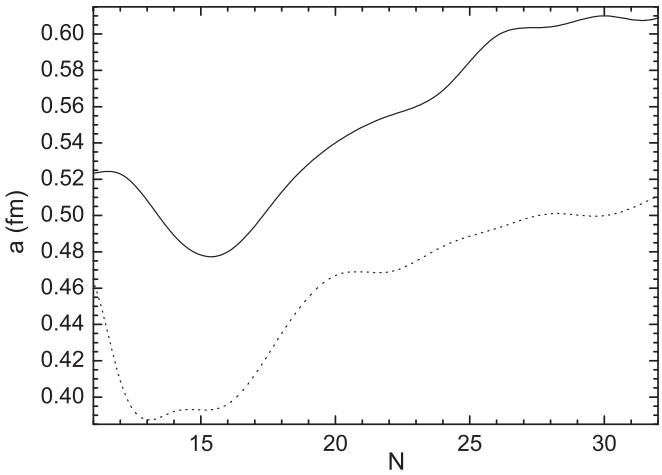

FIG. 7. The comparison of isotopic dependencies of diffuseness of spherical Mg obtained with method I (solid line) and method II (dotted line). The values of a are obtained at $\rho_0 = 0.16$ fm^{-3}.

is responsible for the peculiarities in isotopic dependence of the nuclear diffuseness. The same was pointed out in Ref. [20].

The dependencies of a on N in Figs. 7–11 are rather complicated to be fit with a simple formula. As in Refs. [21,50], one can consider the dependence of a on the neutron separation energy S_n. Indeed, the value of a is proportional to $1/\sqrt{S_n}$. In this case one can suggest the simple parametrization

$$a(N) = a_0 \frac{N}{2N - N_0} \sqrt{S_0/S_n}\ \text{(fm)}, \tag{26}$$

where a_0 and S_0 are the diffuseness and neutron separation energy, respectively, in the isotope with neutron number N_0. As seen in Figs. 8 and 9, this expression allows us to estimate a diffuseness with satisfactory accuracy. Although the value of N_0 can be arbitrary chosen, we set $N_0 = Z$ in Figs. 8 and 9. Expression (26) provides a better evaluation of a for N closer

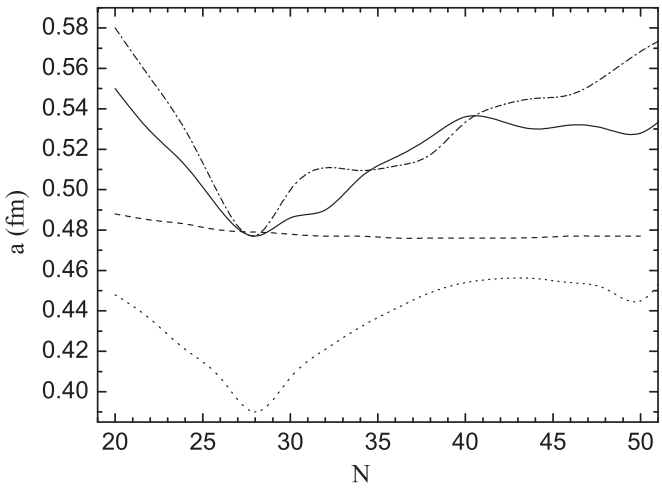

FIG. 8. The same as in Fig. 7, but for spherical Ni. The fit of the solid line with Eq. (26) at $N_0 = 28$ is presented by dash-dotted line. The isotopic dependence of a calculated with Eqs. (25) is presented by dashed line.

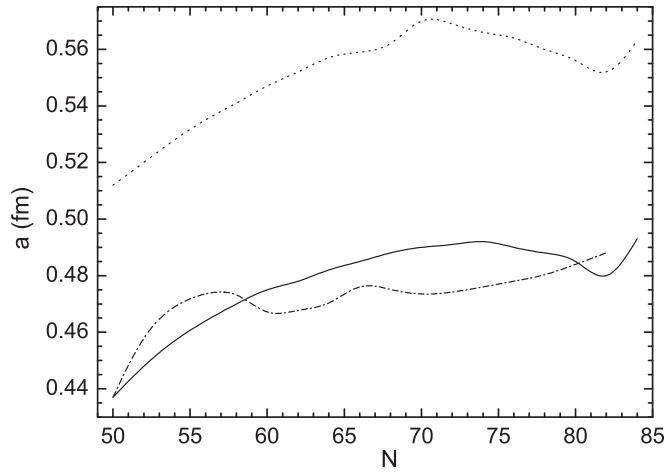

FIG. 9. The same as in Fig. 7, but for spherical Sn. The fit of the solid line with Eq. (26) at $N_0 = 50$ is presented by dash-dotted line.

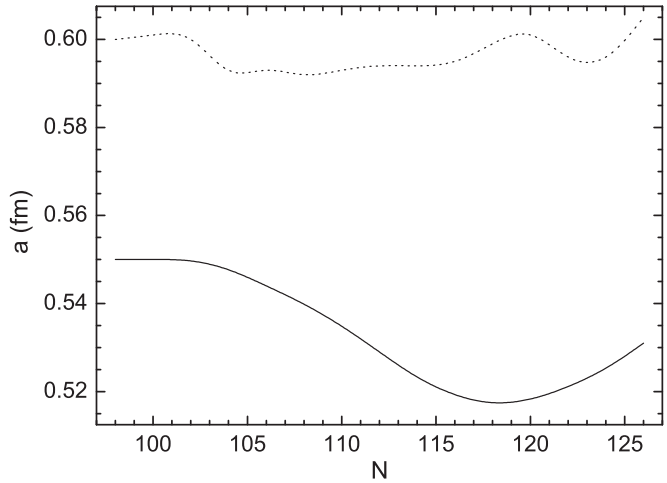

FIG. 10. The same as in Fig. 7, but for spherical Pb.

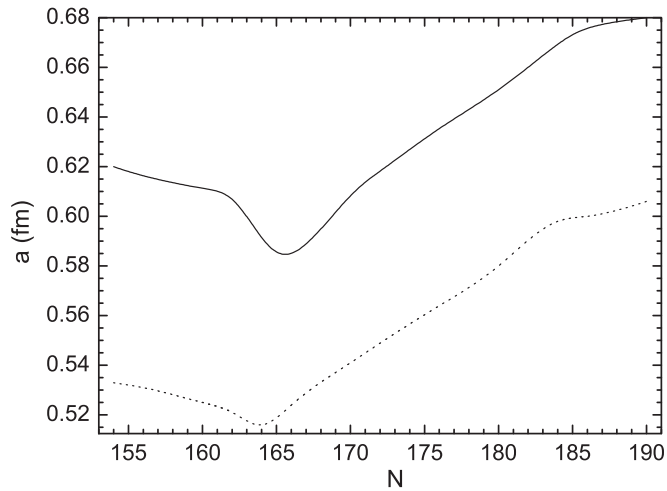

FIG. 11. The same as in Fig. 7, but for spherical Ds.

to N_0 and heavier nuclei. In Fig. 8, the isotopic dependence of $a = (Za_p + Na_n)/A$ is presented, where the values of a_p and a_n are calculated with Eqs. (25). For the most of isotopes, the accuracy of this parametrization is within 15%.

B. Nucleus-nucleus interaction potential

To account properly for the particle number in Eq. (18), we use the scaled strength $C_0 = C_0'\rho_{10}\rho_{20}/\rho_0^2$, where ρ_{10} and ρ_{20} are defined by Eq. (23) for interacting nuclei. The constant $C_0' = 339$ MeV/fm^3 is related to $\rho_0 = 0.16$ fm^{-3} [25], the parameters F_{ex}, α, σ, and γ are chosen such that nuclear properties are described. The NN interaction corresponding to Eq. (18) is

$$F = \frac{\delta^2 \mathcal{E}^{\rm v}_{\rm norm}(x)}{\delta x^2} = C_0 \frac{F_{ex}}{2(1+\gamma x)^3}\{2 + 2\alpha x^\sigma + \alpha\sigma x^\sigma(1+\gamma x)[3+\sigma+\gamma x(1+\sigma)]\}. \quad (27)$$

This expression is obtained by taking the second derivative of Eq. (18) with respect to x. At $x \to 0$ we get external NN interaction and $F \to C_0 F_{ex}$. The NN interaction at saturation density is found for $x \to 1$.

Varying the parameters in Eq. (27), one can obtain different forms of the NN interaction. For example, at $\gamma = 0$ and $\sigma = 1$,

$$F = C_0[F_{ex} + (F_{in} - F_{ex})x] \quad (28)$$

has the Migdal form [25] with $F_{in} = F_{ex}(1 + 3\alpha)$.

The nucleus-nucleus interaction potential V is represented as the sum [23]

$$V(R) = V_{\rm C}(R) + V_N(R) + V_R(R) \quad (29)$$

of the Coulomb $V_{\rm C}$, nuclear V_N, and centrifugal potentials. While $V_{\rm C}$ and V_R have the analytical forms, the calculation of the potential $V_N(R)$ is the most difficult. We calculate it in accordance with the double-folding procedure as

$$V_N(R) = \int d\mathbf{r_1} d\mathbf{r_2}\, \rho_1(\mathbf{r_1})\rho_2(\mathbf{R} - \mathbf{r_2})F(\mathbf{r_2} - \mathbf{r_1}). \quad (30)$$

The effective NN forces, Eq. (28),

$$F(\mathbf{r_2} - \mathbf{r_1}) = C_0\{F_{in}x(\mathbf{r_1}) + F_{ex}[1 - x(\mathbf{r_1})]\}\delta(\mathbf{r_2} - \mathbf{r_1}), \quad (31)$$

depend on the total nuclear density $\rho(\mathbf{r_1}) = \rho_1(\mathbf{r_1}) + \rho_2(\mathbf{R} - \mathbf{r_2})$. The interaction strengths are defined by the Landau–Migdal parameters $F_{in} = 0.09$ and $F_{ex} = -2.59$, $C_0 = 300$ MeV fm^3 ($\rho_0 = 0.17$ fm^3) were determined from a fit to experimentally measured properties of nuclei [25]. The values employed in our previous calculations with Eq. (31) fell within the range $r_0 = 1.15$–1.16 fm for the nuclear radii and within the range $a = 0.53$–0.56 fm for the diffuseness parameters, depending on the nuclear mass. For the α particle, $r_0 = 1.01$ fm and $a = 0.47$ fm were used. These values allow us to describe rather well the height V_B of the Coulomb barriers in various reactions. However, in several reactions the Coulomb barriers are underestimated in our calculations. For example, in the ^{58}Ni $+^{58}$Ni reaction the calculated V_B was about 3 MeV smaller than the experimental value. As shown, for example in Ref. [23], the tail of the total nucleon density ρ mainly influence the value of V_N. The role of ρ_1 is less important because its contribution to V_N is proportional to $(N - Z)/A$.

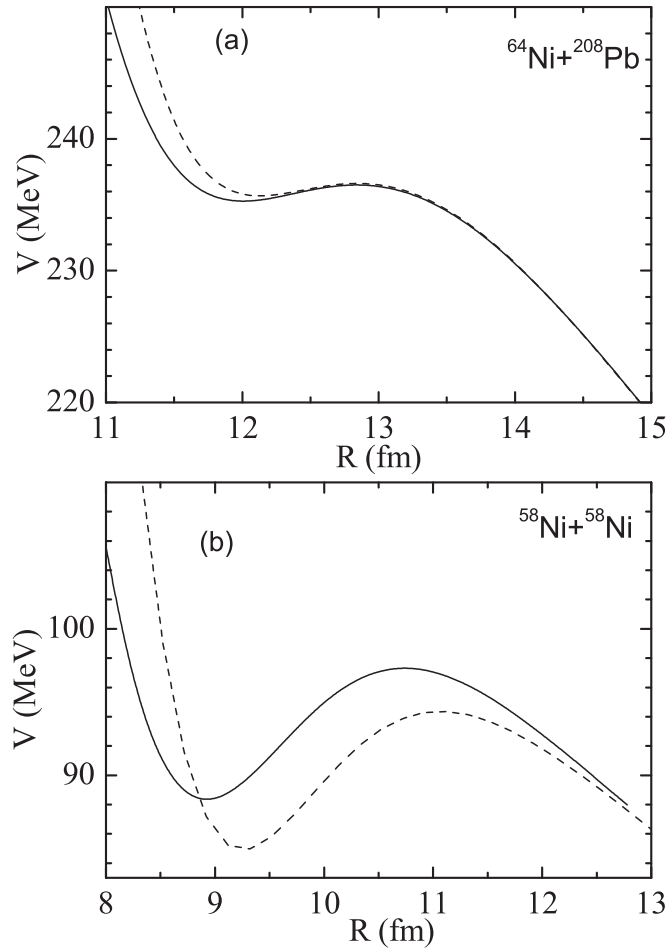

FIG. 12. Comparison of nucleus-nucleus potentials calculated with Eq. (27) and using nucleon densities of method I (solid lines), and with Eq. (31) and adopted ρ (dashed lines) for the reactions indicated. The parameters are given in the text.

As seen, the values of a and r_0 found in the present work are smaller than those used in our previous calculations of the nucleus-nucleus potential with Eq. (31). If they were used with the interaction (31), the Coulomb barrier barrier would be higher than those resulting from the experimental data. By using the values of a and r_0 found, we calculate the nucleus-nucleus potential with F defined in the general form (27). As in Ref. [26], we set $\sigma = 1/3$ and look for the values of F_{ex}, α, and γ which provide a good description of the Coulomb barrier heights.

As found, with $F_{ex} = -10.8$, $\alpha = -0.534$, $\gamma = 0.4$, and nucleon densities obtained with method I, the calculated nucleus-nucleus potentials provide correct values of the Coulomb barrier height and are close to those obtained with the Migdal interaction (31). In the ^{64}Ni $+^{208}$Pb reaction, the present potential and that calculated previously with Eq. (31) almost coincide (Fig. 12). In the ^{58}Ni $+^{58}$Ni reaction (Fig. 12), the shapes of the potentials are almost the same but the present calculation results in a 3 MeV higher Coulomb barrier that is closer to that required to describe the fusion excitation function at energies near the barrier [51]. Note that the height of the

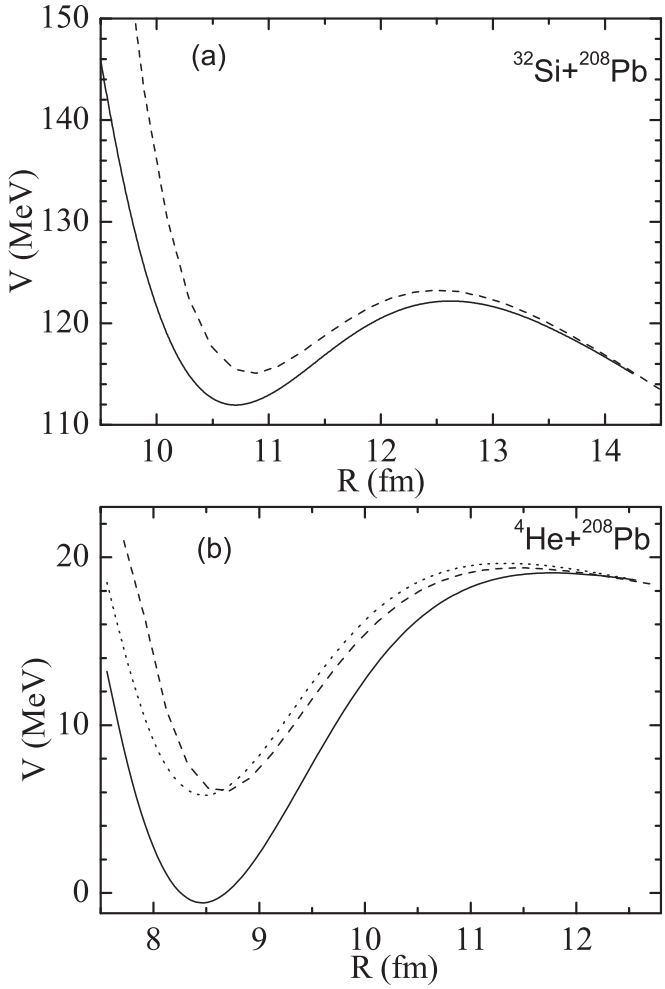

FIG. 13. The same as in Fig. 12, but for the asymmetric reactions indicated. The dotted line is obtained with the same parameters as the solid line, but with $a = 0.39$ fm for ^{4}He.

Coulomb barrier is precisely defined by measuring the fusion excitation function.

With the parameters used we obtain $F_{in} = 0.062$, which is relatively close to the internal constant of the interaction (31). The strength $|F_{ex}|$ of the external nucleon-nucleon interaction is larger than in the Migdal interaction. Indeed, the calculated nucleon density distribution has smaller diffuseness because of the larger nucleon-nucleon attraction used.

For the systems ^{32}S $+^{208}$Pb and ^{4}He $+^{208}$Pb, the nucleus-nucleus potentials obtained with nucleon densities discussed in this paper are quite similar to those calculated with the prescription of Ref. [23] for asymmetric nuclear systems (Fig. 13). The calculations with self-consistent nucleon densities result in 2.3–6.5 MeV deeper potential pocket in the nucleus-nucleus potential and in slightly smaller height, 0.3–1 MeV, of the Coulomb barrier. Because we did not calculate the diffuseness for ^{4}He, the sensitivity of the results to its variation is demonstrated in Fig. 13.

IV. SUMMARY

Two energy density functional methods were applied for obtaining the nucleon density distributions in spherical nuclei. One of them is partially *ab initio* method based on Ref. [11]. The second, the Fayans EDF method [5,26,27], is completely phenomenological. The nucleon density profiles were fit with the Fermi-type expression and the isotopic dependencies of its parameters were explored. The isotopic dependence of the parameter of the nuclear radius is found to be weak, while the value of the nuclear diffuseness quite strongly depends on the neutron number. If the neutron shell is closed by the level with large orbital angular momentum, the dependence $a(N)$ would have a minimum at this magic number. Thus, the centrifugal barrier for nucleons suppresses the diffuseness of nuclear surface. The simple parametrization of $a(N)$, which is proportional to $1/\sqrt{S_n}$, was suggested.

As shown, the value of the diffuseness is related to the attraction strength (the external constant F_{ex}) of the NN interaction. The external constant of the density-dependent NN forces mainly predetermines the height of the Coulomb barrier, which is a measurable value. The nucleus-nucleus potential is defined by the density-dependent NN interaction and nucleon density profiles. The calculation with larger diffuseness and smaller $|F_{ex}|$ could result in the same barrier height as the calculation with smaller a and larger $|F_{ex}|$. Thus, if the parameters of the EDF or of the corresponding effective NN interaction were fit to nuclear ground-state characteristics, one should check whether this interaction is able to reproduce the height of the Coulomb barrier between two interacting nuclei.

ACKNOWLEDGMENTS

This work was supported in part by the DFG (Bonn) and RFBR (Moscow). G.G.A. and N.V.A. acknowledge the support from the Alexander von Humboldt-Stiftung (Bonn). E.E.S. and S.V.T. thank the Russian Science Foundation (Grants No. 16-12-10155 and No. 16-12-10161) and the RFBR (Grants No. 14-02-00107-a, No. 14-22-03040_ofi-m, and No. 16-02-00228) for support.

[1] P. Maris, A. M. Shirokov, and J. P. Vary, Phys. Rev. C **81**, 021301 (2010).
[2] U.-G. Meißner, Nucl. Phys. A **928**, 64 (2014).
[3] D. Vautherin and D. M. Brink, Phys. Rev. C **5**, 626 (1972).
[4] J. Dechargé and D. Gogny, Phys. Rev. C **21**, 1568 (1980).
[5] A. V. Smirnov, S. V. Tolokonnikov, and S. A. Fayans, Sov. J. Nucl. Phys. **48**, 995 (1988).
[6] V. A. Khodel and E. E. Saperstein, Phys. Rep. **92**, 183 (1982).
[7] M. Bender, P.-H. Heenen, and P.-G. Reinhard, Rev. Mod. Phys. **75**, 121 (2003).
[8] P. Ring, Prog. Part. Nucl. Phys. **37**, 193 (1996).

[9] G. A. Lalazissis, D. Vretenar, and P. Ring, Phys. Rev. C **57**, 2294 (1998).
[10] J. Meng, H. Toki, S. G. Zhou, S. Q. Zhang, W. H. Long, and L. S. Geng, Prog. Part. Nucl. Phys. **57**, 470 (2006).
[11] F. Hofmann and H. Lenske, Phys. Rev. C **57**, 2281 (1998).
[12] M. Baldo, P. Schuck, and X. Viñas, Phys. Lett. B **663**, 390 (2008).
[13] M. Baldo, L. M. Robledo, P. Schuck, and X. Viñas, Phys. Rev. C **87**, 064305 (2013).
[14] X. Viñas, M. Centelles, X. Roca-Maza, and M. Warda, AIP Conf. Proc. **1491**, 101 (2012).
[15] L.-W. Chen, C. M. Ko, and B.-A. Li, Phys. Rev. C **72**, 064309 (2005).
[16] C. J. Horowitz and J. Piekarewicz, Phys. Rev. Lett. **86**, 5647 (2001).
[17] V. Yu. Denisov and V. A. Nesterov, Phys. At. Nucl. **65**, 814 (2002).
[18] M. K. Gaidarov, A. N. Antonov, P. Sarriguren, and E. Moya de Guerra, Phys. Rev. C **84**, 034316 (2011).
[19] M. K. Gaidarov, A. N. Antonov, P. Sarriguren, and E. Moya de Guerra, J. Phys.: Conf. Ser. **533**, 012016 (2014).
[20] M. Warda, M. Centelles, X. Vinas, and X. Roca-Maza, Phys. Rev. C **89**, 064302 (2014).
[21] G. Scamps, D. Lacroix, G. G. Adamian, and N. V. Antonenko, Phys. Rev. C **88**, 064327 (2013); G. G. Adamian, N. V. Antonenko, L. A. Malov, G. Scamps, and D. Lacroix, *ibid.* **90**, 034322 (2014).
[22] I. Dutt and R. K. Puri, Phys. Rev. C **81**, 047601 (2010).
[23] G. G. Adamian *et al.*, Int. J. Mod. Phys. E **05**, 191 (1996).
[24] V. Yu. Denisov and V. A. Nesterov, Phys. At. Nucl. **69**, 1472 (2006).
[25] A. B. Migdal, *Theory of Finite Fermi Systems and Applications to Atomic Nuclei* (Wiley, New York, 1967).
[26] S. A. Fayans, S. V. Tolokonnikov, E. L. Trykov, and D. Zawischa, Nucl. Phys. A **676**, 49 (2000).
[27] S. V. Tolokonnikov and E. E. Saperstein, Phys. At. Nucl. **73**, 1684 (2010).
[28] J. W. Negele and D. Vautherin, Phys. Rev. C **5**, 1472 (1972).
[29] J. C. Bernauer, M. O. Distler, J. Friedrich, T. Walcher, P. Achenbach, C. Ayerbe Gayoso, R. Böhm, D. Bosnar, L. Debenjak, L. Doria, A. Esser, H. Fonvieille, M. Gómez Rodríguez dela Paz, J. M. Friedrich, M. Makek, H. Merkel, D. G. Middleton, U. Müller, L. Nungesser, J. Pochodzalla, M. Potokar, S. Sánchez Majos, B. S. Schlimme, S. Sirca, and M. Weinriefer, Phys. Rev. C **90**, 015206 (2014).
[30] T. R. Gentile and C. B. Crawford, Phys. Rev. C **83**, 055203 (2011).
[31] H. Lenske and C. Fuchs, Phys. Lett. B **345**, 355 (1995).
[32] G. Dahlquist and Ã. Björck, *Numerical Methods* (Prentice-Hall, Englewoods Cliffs, 1974).
[33] G. Audi, M. Wang, A. H. Wapstra, F. G. Kondev, M. MacCormick, and X. Xu, Nucl. Data Sheets **120**, 1 (2014).
[34] R. N. Bernard and M. Anguiano, Nucl. Phys. A **953**, 32 (2016).
[35] N. Tsoneva and H. Lenske, Phys. Rev. C **77**, 024321 (2008).
[36] N. Tsoneva and H. Lenske, Phys. Lett. B **695**, 174 (2011).
[37] H. De Vries, C. W. De Jager, and C. De Vries, At. Data Nucl. Data Tables **36**, 495 (1987).
[38] S. V. Tolokonnikov, S. Kamerdzhiev, D. Voitenkov, S. Krewald, and E. E. Saperstein, Phys. Rev. C **84**, 064324 (2011).
[39] E. E. Saperstein and S. V. Tolokonnikov, Phys. At. Nucl. **74**, 1277 (2011).
[40] S. A. Fayans, JETP Lett. **68**, 169 (1998).
[41] B. Friedman and V. R. Pandharipande, Nucl. Phys. A **361**, 502 (1981).
[42] I. N. Borzov, E. E. Saperstein, and S. V. Tolokonnikov, Phys. At. Nucl. **71**, 469 (2008).
[43] I. N. Borzov, E. E. Saperstein, S. V. Tolokonnikov, G. Neyens, and N. Severijns, Eur. Phys. J. A **45**, 159 (2010).
[44] S. V. Tolokonnikov, S. Kamerdzhiev, S. Krewald, E. E. Saperstein, and D. Voitenkov, Eur. Phys. J. A **48**, 70 (2012).
[45] S. Kamerdzhiev, S. Krewald, S. Tolokonnikov, E. E. Saperstein, and D. Voitenkov, EPJ Web Conf. **38**, 10002 (2012).
[46] S. V. Tolokonnikov, S. Kamerdzhiev, S. Krewald, E. E. Saperstein, and D. Voitenkov, EPJ Web Conf. **38**, 04002 (2012).
[47] N. V. Gnezdilov, I. N. Borzov, E. E. Saperstein, and S. V. Tolokonnikov, Phys. Rev. C **89**, 034304 (2014).
[48] R. A. Kuzyakin, V. V. Sargsyan, G. G. Adamian, N. V. Antonenko, E. E. Saperstein, and S. V. Tolokonnikov, Phys. Rev. C **85**, 034612 (2012).
[49] V. G. Soloviev, *Theory of Atomic Nuclei: Quasiparticles and Phonons* (Institute of Physics Publishing, Bristol and Philadelphia, 1992).
[50] T. M. Shneidman, G. G. Adamian, N. V. Antonenko, R. V. Jolos, and W. Scheid, Phys. Rev. C **67**, 014313 (2003).
[51] V. V. Sargsyan, G. G. Adamian, N. V. Antonenko, W. Scheid, and H. Q. Zhang, Phys. Rev. C **84**, 064614 (2011).